Weierstraß-Institut
für Angewandte Analysis und Stochastik

im Forschungsverbund Berlin e.V.

Preprint ISSN 0946 – 8633

A regularized Newton method in electrical impedance tomography using shape Hessian information

Karsten Eppler[1] and Helmut Harbrecht[2]

submitted: 18 Jun 2004

[1] Weierstraß Institut für Angewandte Analysis und Stochastik, Mohrenstr. 39, 10117 Berlin, Germany, E-Mail: eppler@wias-berlin.de

[2] Institut für Informatik und Praktische Mathematik, Christian–Albrechts–Universität zu Kiel, Olshausenstr. 40, 24098 Kiel, Germany. E-Mail: hh@numerik.uni-kiel.de

No. 943

Berlin 2004

2000 *Mathematics Subject Classification.* 49Q10, 49M37, 65N38, 49K20.

Key words and phrases. electrical impedance tomography, shape optimization, integral equation method, Newton type descent.

This research has been carried out when the second author stayed at the Department of Mathematics, University Utrecht, Netherlands, supportet by the EU-IHP project *Nonlinear Approximation and Adaptivity: Breaking Complexity in Numerical Modelling and Data Representation.*

Edited by
Weierstraß-Institut für Angewandte Analysis und Stochastik (WIAS)
Mohrenstraße 39
10117 Berlin
Germany

Fax: + 49 30 2044975
E-Mail: preprint@wias-berlin.de
World Wide Web: http://www.wias-berlin.de/

ABSTRACT. The present paper is concerned with the identification of an obstacle or void of different conductivity included in a two-dimensional domain by measurements of voltage and currents at the boundary. We employ a reformulation of the given identification problem as a shape optimization problem as proposed by Sokolowski and Roche [20]. It turns out that the shape Hessian degenerates at the given hole which gives a further hint on the ill-posedness of the problem. For numerical methods, we propose a preprocessing for detecting the barycenter and a crude approximation of the void or hole. Then, we resolve the shape of the hole by a regularized Newton method.

INTRODUCTION

Let $D \subset \mathbb{R}^2$ denote a bounded domain with boundary $\partial D = \Sigma$ and assume the existence of a simply connected subdomain $S \subset D$, consisting of material with constant conductivity, essentially different from the likewise constant conductivity of the material in the subregion $\Omega = D \setminus \overline{S}$. We consider the identification problem of this inclusion if the Cauchy data of the electrical potential u are measured at the boundary Σ , i.e., if a single pair $f = u|_\Sigma$ and $g = (\partial u/\partial \mathbf{n})|_\Sigma$ is known.

The problem under consideration is a special case of the general conductivity reconstruction problem and is severely ill-posed. It has been intensively investigated as an inverse problem. We refer for example to Hettlich and Rundell [16] for numerical algorithms and to Friedmann and Isakov [12] as well as Alessandrini, Isakov and Powell [1] for particular results concerning uniqueness. Moreover, we refer to Brühl and Hanke [2, 3] for methods using the complete Dirichlet–to–Neumann operator at the outer boundary. We emphasize that we focus in the present paper on exact measurements and do not consider noisy data.

In [20], Roche and Sokolowski have been introduced a formulation as shape optimization problem. Moreover, analysis and numerical results are presented for first order shape optimization algorithms. In the present paper we investigate related second order methods, developed and applied by the authors in [8, 9, 10]. Provided that the interface $\Gamma = \partial S$ is sufficiently regular, higher order smoothness for the objective can be shown by means of standard results. We assume the inclusion to be starshaped with respect to a given pole $\mathbf{x}_0 \in D$ and derive the second order shape derivatives in terms of polar coordinates. Nevertheless, we prove compactness of the shape Hessian at the optimal domain $\Omega^\star = D \setminus \overline{S^\star}$. This degeneration is completely different from the regular coercive situations observed in [9, 10]. Hence, neither the validity of a sufficient second order condition nor a quadratic convergence of the Newton method can be guaranteed.

Using finite Fourier series to represent the boundary of the inclusion we arrive at a finite dimensional optimization problem. This optimization problem will be minimized by a Newton method which has to be regularized due to the compactness of the shape Hessian at the optimal domain. Precisely, we employ a Tikhinov regularization of the necessary optimality condition. By numerical experiments we show that our method outperforms first order algorithms. Introducing a preprocessing for detecting the barycenter and a first crude approximation of the inclusion, we are able extend our approach also to the case of small inclusions without knowing the pole in advance.

The present paper is organized as follows. In Section 1 we present the physical model and reformulate the identification problem as shape optimization problem. We compute the gradient and the Hessian of the given shape functional. Then, in Section 2, we analyze the shape Hessian and prove its degeneration at the optimal domain. In Section 3 we discretize the boundary of the inclusion and replace the infinite dimensional optimization problem by finite dimensional one. Moreover, we propose a boundary element method to compute the shape functional as well as its gradient and Hessian. In Section 4, we perform several numerical experiments to compare the regularized Newton method with a quasi Newton method. In the last section, that is Section 5, we state concluding remarks.

1. Shape problem formulation

1.1. **The physical model.** Let $D \in \mathbb{R}^2$ be a simply connected domain with boundary $\Sigma = \partial D$ and assume that an unknown simply connected inclusion S with regular boundary $\Gamma = \partial S$ is located inside the domain D satisfying $\operatorname{dist}(\Sigma, \Gamma) > 0$, cf. Figure 1.1. To determine the inclusion S we measure for a given current distribution $g \in H^{-1/2}(\Sigma)/\mathbb{R}$ the voltage distribution $f \in H^{1/2}(\Sigma)$ at the boundary Σ. Hence, we are seeking a domain $\Omega := D \setminus \overline{S}$ and an associated harmonic function u, satisfying the system of equations

$$\begin{aligned} \Delta u &= 0 && \text{in } \Omega, \\ u &= 0 && \text{on } \Gamma, \\ u &= f && \text{on } \Sigma, \\ \frac{\partial u}{\partial \mathbf{n}} &= g && \text{on } \Sigma. \end{aligned}$$

This system denotes an overdetermined boundary value problem which admits a solution only for the true inclusion S.

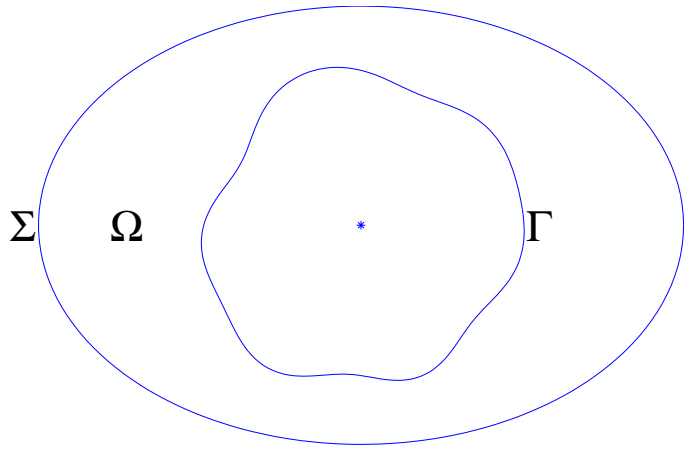

FIGURE 1.1. The domain Ω and its boundaries Γ and Σ.

Following Sokolowski and Roche [20], we introduce the auxiliary harmonical functions v and w satisfying

$$\begin{aligned} \Delta v &= 0 & \Delta w &= 0 & &\text{in } \Omega, \\ v &= 0 & w &= 0 & &\text{on } \Gamma, \\ \frac{\partial v}{\partial \mathbf{n}} &= g & w &= f & &\text{on } \Sigma, \end{aligned} \tag{1.1}$$

and consider the following shape optimization problem

$$J(\Omega) = \int_\Omega \|\nabla(v-w)\|^2 d\mathbf{x} = \int_\Sigma \left(g - \frac{\partial w}{\partial \mathbf{n}}\right)(v-f)d\sigma \to \inf . \tag{1.2}$$

Herein, the infimum has to be taken over all domains including a void with sufficiently regular boundary. We refer to Roche and Sokolowski [20] for the existence of optimal solutions with respect to this shape optimization problem.

1.2. **Shape calculus.** For sake of clearness in representation, we repeat the shape calculus concerning the problem under consideration by means of boundary variations. The shape gradient has been computed first in [20] while the structure of the shape Hessian has been sketched in terms of material derivatives. But we emphasize that we derive a boundary integral representation of the shape Hessian which allows us to investigate and implement it. For a survey on the shape calculus based on the material derivative concept, we refer the reader to Sokolowski and Zolesio [21] and the references therein.

Let the underlying variation fields $\mathbf{V}$ be sufficiently smooth such that $C^{2,\alpha}$-regularity is preserved for all perturbed domains. Moreover, for sake of simplicity, we assume in addition that the outer boundary and the measurements are sufficiently regular

such that the state functions $v = v(\Omega)$ and $w = w(\Omega)$ satisfy

$$v, w \in C^{2,\alpha}(\Omega). \tag{1.3}$$

Then, a formal differentiation of (1.2) in terms of local derivatives yields immediately

$$dJ(\Omega)[\mathbf{V}] = \int_\Gamma \langle \mathbf{V}, \mathbf{n}\rangle \|\nabla(v-w)\|^2 d\sigma + 2\int_\Omega \langle \nabla(v-w), \nabla(dv-dw)\rangle d\mathbf{x},$$

where the local shape derivatives $dv = dv[\mathbf{V}]$ and $dw = dw[\mathbf{V}]$ satisfy

$$\begin{aligned} \Delta dv &= 0 & \Delta dw &= 0 & &\text{in } \Omega, \\ dv &= -\langle \mathbf{V}, \mathbf{n}\rangle \frac{\partial v}{\partial \mathbf{n}} & dw &= -\langle \mathbf{V}, \mathbf{n}\rangle \frac{\partial w}{\partial \mathbf{n}} & &\text{on } \Gamma, \\ \frac{\partial dv}{\partial \mathbf{n}} &= 0 & dw &= 0 & &\text{on } \Sigma, \end{aligned} \tag{1.4}$$

Using $\partial\Omega = \Gamma \cup \Sigma$ and the known boundary data from (1.1) and (1.4), the boundary integral representation of the shape gradient is obtained via repeated integration by parts

$$\begin{aligned} dJ(\Omega)[\mathbf{V}] &= \int_\Gamma \langle \mathbf{V}, \mathbf{n}\rangle \|\nabla(v-w)\|^2 d\sigma + 2\int_{\partial\Omega} (dv-dw)\frac{\partial(v-w)}{\partial \mathbf{n}} d\sigma \\ &= 2\int_\Sigma dv \frac{\partial(v-w)}{\partial \mathbf{n}} d\sigma - \int_\Gamma \langle \mathbf{V}, \mathbf{n}\rangle \left(\frac{\partial(v-w)}{\partial \mathbf{n}}\right)^2 d\sigma \end{aligned}$$

Furthermore, we conclude from

$$\begin{aligned} 0 &= -\int_\Omega v\Delta dv d\mathbf{x} + \int_{\partial\Omega} v\frac{\partial dv}{\partial \mathbf{n}} d\sigma = \int_\Omega \langle \nabla dv, \nabla v\rangle d\mathbf{x} \\ &= -\int_\Omega dv\Delta v d\mathbf{x} + \int_{\partial\Omega} dv\frac{\partial v}{\partial \mathbf{n}} d\sigma, \end{aligned}$$

and likewise

$$\begin{aligned} 0 &= -\int_\Omega w\Delta dv d\mathbf{x} + \int_{\partial\Omega} w\frac{\partial dv}{\partial \mathbf{n}} d\sigma = \int_\Omega \langle \nabla dv, \nabla w\rangle d\mathbf{x} \\ &= -\int_\Omega dv\Delta w d\mathbf{x} + \int_{\partial\Omega} dv\frac{\partial w}{\partial \mathbf{n}} d\sigma, \end{aligned}$$

the relations

$$\int_\Sigma dv\frac{\partial v}{\partial \mathbf{n}} d\sigma = \int_\Gamma \langle \mathbf{V}, \mathbf{n}\rangle \left(\frac{\partial v}{\partial \mathbf{n}}\right)^2 d\sigma, \qquad \int_\Sigma dv\frac{\partial w}{\partial \mathbf{n}} d\sigma = \int_\Gamma \langle \mathbf{V}, \mathbf{n}\rangle \frac{\partial v}{\partial \mathbf{n}}\frac{\partial w}{\partial \mathbf{n}} d\sigma.$$

Consequently, the shape gradient reads as

$$dJ(\Omega)[\mathbf{V}] = \int_\Gamma \langle \mathbf{V}, \mathbf{n}\rangle \left[\left(\frac{\partial v}{\partial \mathbf{n}}\right)^2 - \left(\frac{\partial w}{\partial \mathbf{n}}\right)^2\right] d\sigma, \tag{1.5}$$

see also [20]. Note that, as an immediate consequence of the shape calculus, (1.5) implies an simplified first order necessary condition

$$\frac{\partial v}{\partial \mathbf{n}}\Big|_\Gamma \equiv \frac{\partial w}{\partial \mathbf{n}}\Big|_\Gamma. \tag{1.6}$$

In the case of a starshaped hole S, the boundary $\Gamma = \partial S$ can be parametrized by a function $r = r(\varphi)$ of the polar angle φ and the perturbation field $\mathbf{V}$ can be chosen as $\mathbf{V} = dr(\varphi)\mathbf{e}_r(\varphi)$ with respect to a pole inside S. Hence, the shape gradient $dJ[dr]$ can be expressed equivalently in local coordinates as

$$dJ(\Omega)[dr] = \int_0^{2\pi} dr(\varphi)\, r(\varphi) \left[\left(\frac{\partial w}{\partial \mathbf{n}}\right)^2 - \left(\frac{\partial v}{\partial \mathbf{n}}\right)^2 \right](\varphi)\, d\varphi, \tag{1.7}$$

where the minus sign issues from the fact that $\langle \mathbf{e}_r, \mathbf{n}\rangle = -r/\sqrt{r^2 + r'^2}$.

To derive the shape Hessian, we proceed similar to [6, 7] by differentiating the shape gradient (1.7) and arrive at

$$\begin{aligned} d^2J(\Omega)[dr_1, dr_2] = \int_0^{2\pi} & dr_1(\varphi)\, dr_2(\varphi) \left\{ \|\nabla w\|^2 - \|\nabla v\|^2 \right\} \\ & + dr_1(\varphi)\, dr_2(\varphi)\, r(\varphi) \frac{\partial}{\partial \mathbf{e}_r} \left\{ \|\nabla w\|^2 - \|\nabla v\|^2 \right\} \\ & + 2dr_1(\varphi)\, r(\varphi) \left\{ \frac{\partial w}{\partial \mathbf{n}} \frac{\partial dw[dr_2]}{\partial \mathbf{n}} - \frac{\partial v}{\partial \mathbf{n}} \frac{\partial dv[dr_2]}{\partial \mathbf{n}} \right\} d\varphi, \end{aligned} \tag{1.8}$$

where all data have to be understood as traces on the unknown boundary Γ.

The homogeneous Dirichlet data $v|_\Gamma = 0$ imply the identity

$$(\|\nabla v\|^2)|_\Gamma = \left(\frac{\partial v}{\partial \mathbf{n}}\right)^2.$$

Moreover, observing $\partial/\partial \mathbf{t} = -\partial/\partial \phi$, we can decompose

$$\frac{\partial}{\partial \mathbf{e}_r}\left(\|\nabla v\|^2\right) = \frac{2}{\sqrt{r^2 + r'^2}} \frac{\partial v}{\partial \mathbf{n}} \left\{ r \frac{\partial^2 v}{\partial \mathbf{n}^2} - r' \frac{\partial^2 v}{\partial \mathbf{n} \partial \mathbf{t}} \right\}.$$

Since v is harmonical admitting homogeneous Dirichlet data on Γ, we arrive at the identity

$$\frac{\partial^2 v}{\partial \mathbf{n}^2} = -\kappa \frac{\partial v}{\partial \mathbf{n}},$$

where κ denotes the curvature with respect to Γ, see [9] for the details.

Since analogous results are valid with respect to w, we can simplify (1.8) by

$$
\begin{aligned}
(1.9)\qquad d^2 J(\Omega)[dr_1, dr_2] = \int_0^{2\pi} dr_1\, dr_2 \Bigg\{ & \frac{2rr'}{\sqrt{r^2+r'^2}} \left[\frac{\partial v}{\partial \mathbf{n}} \frac{\partial^2 v}{\partial \mathbf{n} \partial \mathbf{t}} - \frac{\partial w}{\partial \mathbf{n}} \frac{\partial^2 w}{\partial \mathbf{n} \partial \mathbf{t}} \right] \\
& + \left(1 - \frac{2r^2\kappa}{\sqrt{r^2+r'^2}} \right) \left[\left(\frac{\partial w}{\partial \mathbf{n}} \right)^2 - \left(\frac{\partial v}{\partial \mathbf{n}} \right)^2 \right] \Bigg\} \\
& + 2 dr_1\, r \left\{ \frac{\partial w}{\partial \mathbf{n}} \frac{\partial dw[dr_2]}{\partial \mathbf{n}} - \frac{\partial v}{\partial \mathbf{n}} \frac{\partial dv[dr_2]}{\partial \mathbf{n}} \right\} d\varphi.
\end{aligned}
$$

2. Analyzing the shape Hessian

2.1. **Boundary integral equations.** In this subsection we compute the unknown boundary data of the state functions v and w by boundary integral equations. We introduce the single layer and the double layer operator with respect the boundaries $\Phi, \Psi \in \{\Gamma, \Sigma\}$ by

$$
\begin{aligned}
(V_{\Phi\Psi} u)(\mathbf{x}) &:= -\frac{1}{2\pi} \int_\Phi \log \|\mathbf{x}-\mathbf{y}\| u(\mathbf{y}) d\sigma_\mathbf{y}, \qquad \mathbf{x} \in \Psi, \\
(K_{\Phi\Psi} u)(\mathbf{x}) &:= \frac{1}{2\pi} \int_\Phi \frac{\langle \mathbf{x}-\mathbf{y}, \mathbf{n}_\mathbf{y} \rangle}{\|\mathbf{x}-\mathbf{y}\|^2} u(\mathbf{y}) d\sigma_\mathbf{y}, \qquad \mathbf{x} \in \Psi.
\end{aligned}
$$

Note that $V_{\Phi\Psi}$ denotes an operator of order -1 if $\Phi = \Psi$, i.e. $V_{\Phi\Phi} : H^{-1/2}(\Phi) \to H^{1/2}(\Phi)$, while it is an arbitrarily smoothing compact operator if $\Phi \neq \Psi$ since $\operatorname{dist}(\Gamma, \Sigma) > 0$. Likewise, if $\Sigma, \Gamma \in C^2$, the double layer operator $K_{\Phi\Phi} : H^{1/2}(\Phi) \to H^{1/2}(\Phi)$ is compact while it smoothes arbitrarily if $\Phi \neq \Psi$. We refer the reader to [15, 18] for a detailed description of boundary integral equations.

For sake of simplicity we suppose that $\operatorname{diam} \Omega < 1$ to ensure that $V_{\Phi\Phi}$ is invertible, cf. [17]. Moreover, the canonical spaces of the normal derivatives $(\partial w/\partial \mathbf{n})|_\Gamma$ and $(\partial w/\partial \mathbf{n})|_\Sigma$ contain no constant functions, i.e., $(\partial w/\partial \mathbf{n})|_\Gamma \in H^{-1/2}(\Gamma)/\mathbb{R}$ and $(\partial w/\partial \mathbf{n})|_\Sigma \in H^{-1/2}(\Sigma)/\mathbb{R}$, respectively, and likewise for $(\partial v/\partial \mathbf{n})|_\Gamma$. Then, the normal derivative of w is given by the Dirichlet-to-Neumann map

$$
(2.10)\qquad \begin{bmatrix} V_{\Gamma\Gamma} & V_{\Sigma\Gamma} \\ V_{\Gamma\Sigma} & V_{\Sigma\Sigma} \end{bmatrix} \begin{bmatrix} \frac{\partial w}{\partial \mathbf{n}}\big|_\Gamma \\ \frac{\partial w}{\partial \mathbf{n}}\big|_\Sigma \end{bmatrix} = \begin{bmatrix} 1/2 + K_{\Gamma\Gamma} & K_{\Sigma\Gamma} \\ K_{\Gamma\Sigma} & 1/2 + K_{\Sigma\Sigma} \end{bmatrix} \begin{bmatrix} 0 \\ f \end{bmatrix},
$$

cf. (1.1). Likewise, the unknown boundary data of v are determined by

$$
(2.11)\qquad \begin{bmatrix} V_{\Gamma\Gamma} & -K_{\Sigma\Gamma} \\ -V_{\Gamma\Sigma} & 1/2 + K_{\Sigma\Sigma} \end{bmatrix} \begin{bmatrix} \frac{\partial v}{\partial \mathbf{n}}\big|_\Gamma \\ v|_\Sigma \end{bmatrix} = \begin{bmatrix} 1/2 + K_{\Gamma\Gamma} & -V_{\Sigma\Gamma} \\ -K_{\Gamma\Sigma} & V_{\Sigma\Sigma} \end{bmatrix} \begin{bmatrix} 0 \\ g \end{bmatrix}.
$$

Note that here and in the sequel the operators $(1/2 + K_{\Phi\Phi})$, $\Phi \in \{\Gamma, \Sigma\}$, have to be understood as continuous and bijective operators in terms of $(1/2 + K_{\Phi\Phi}) : H^{1/2}(\Phi)/\mathbb{R} \to H^{1/2}(\Phi)/\mathbb{R}$.

The unknown boundary data of the local shape derivatives $dv = dv[dr]$ and $dw = dw[dr]$ are derived by

$$\begin{bmatrix} V_{\Gamma\Gamma} & V_{\Sigma\Gamma} \\ V_{\Gamma\Sigma} & V_{\Sigma\Sigma} \end{bmatrix} \begin{bmatrix} \frac{\partial dw}{\partial \mathbf{n}}\big|_\Gamma \\ \frac{\partial dw}{\partial \mathbf{n}}\big|_\Sigma \end{bmatrix} = \begin{bmatrix} 1/2 + K_{\Gamma\Gamma} & K_{\Sigma\Gamma} \\ K_{\Gamma\Sigma} & 1/2 + K_{\Sigma\Sigma} \end{bmatrix} \begin{bmatrix} -\langle \mathbf{V}, \mathbf{n}\rangle \frac{\partial w}{\partial \mathbf{n}}\big|_\Gamma \\ 0 \end{bmatrix} \tag{2.12}$$

and

$$\begin{bmatrix} V_{\Gamma\Gamma} & -K_{\Sigma\Gamma} \\ -V_{\Gamma\Sigma} & 1/2 + K_{\Sigma\Sigma} \end{bmatrix} \begin{bmatrix} \frac{\partial dv}{\partial \mathbf{n}}\big|_\Gamma \\ dv|_\Sigma \end{bmatrix} = \begin{bmatrix} 1/2 + K_{\Gamma\Gamma} & -V_{\Sigma\Gamma} \\ -K_{\Gamma\Sigma} & V_{\Sigma\Sigma} \end{bmatrix} \begin{bmatrix} -\langle \mathbf{V}, \mathbf{n}\rangle \frac{\partial v}{\partial \mathbf{n}}\big|_\Gamma \\ 0 \end{bmatrix}. \tag{2.13}$$

2.2. **Compactness of the Hessian at the optimal domain.** Next, we will investigate the shape Hessian at the optimal domain $\Omega^\star$, that is, if the given inclusion is detected and the first order necessary condition (1.6) holds. Consequently, all quantities arising in the considerations are related to the optimal domain $\Omega^\star$ throughout this subsection. Since there holds $v = w$ in (1.1) at $\Omega^\star$, the first two terms in (1.8) vanish and the shape Hessian simplifies according to

$$d^2 J(\Omega^\star)[dr_1, dr_2] = \int_0^{2\pi} 2dr_1(\varphi) r^\star(\varphi) \frac{\partial v}{\partial \mathbf{n}} \left\{ \frac{\partial dw[dr_2]}{\partial \mathbf{n}} - \frac{\partial dv[dr_2]}{\partial \mathbf{n}} \right\} d\varphi. \tag{2.14}$$

Of course, the Hessian $d^2 J(\Omega^\star)$ does *not* vanish since the local shape derivatives $dw[dr_2]$ and $dv[dr_2]$ have prescribed homogeneous Dirichlet and Neumann data at the fixed boundary Σ, respectively (cf. (1.4)). Consequently, we conclude

$$\frac{\partial dv[dr_2]}{\partial \mathbf{n}}\Big|_\Gamma \neq \frac{\partial dw[dr_2]}{\partial \mathbf{n}}\Big|_\Gamma$$

which immediately implies

$$d^2 J(\Omega^\star)[dr_1, dr_2] \neq 0.$$

Nevertheless, for all perturbations dr_2 the Dirichlet data of $dv[dr_2]$ and $dw[dr_2]$ coincide at Γ

$$dv[dr_2]\big|_\Gamma dw[dr_2]\big|_\Gamma == dr_2 r^\star \frac{\partial v}{\partial \mathbf{n}}\Big|_\Gamma.$$

To analyze the shape Hessian, we introduce the multiplication operator

$$Mdr := dr \cdot r^\star \frac{\partial v}{\partial \mathbf{n}}$$

and the operator associated with the difference of the Dirichlet-to-Neumann maps with respect to the Dirichlet data $h[dr] := drr^\star(\partial v/\partial \mathbf{n})|_\Gamma$

$$\Lambda(h[dr]) := \frac{\partial dw[dr]}{\partial \mathbf{n}}\Big|_\Gamma - \frac{\partial dv[dr]}{\partial \mathbf{n}}\Big|_\Gamma.$$

With these operators at hand, we can rewrite (2.14) by

$$d^2 J(\Omega^\star)[dr_1, dr_2] = \langle 2Mdr_1, \Lambda(Mdr_2)\rangle, \tag{2.15}$$

where $\langle \cdot, \cdot \rangle$ denotes the canonical $L^2([0, 2\pi))$-inner product.

Lemma 2.1. *Let* (1.3) *hold, then the multiplication operator*

$$M : H^{1/2}(\Gamma) \to H^{1/2}(\Gamma), \qquad Mdr := dr \cdot r^\star \frac{\partial v}{\partial \mathbf{n}},$$

is continuous.

Proof. Abbreviating $u := r^\star(\partial v/\partial \mathbf{n})|_\Gamma$ we may write $Mdr = dr \cdot u$. Due to results of Triebel [22] or Mazja and Shaposhnikova [19], the multiplication operator M is continuous from $H^{1/2}(\Gamma)$ to $H^{1/2}(\Gamma)$, provided that $u \in C^{0,\alpha}(\Gamma)$ for some $\alpha > 1/2$. From (1.3) we conclude $u = r^\star(\partial v/\partial \mathbf{n})|_\Gamma \in C^{1,\alpha}(\Gamma)$ which implies the assertion. □

Lemma 2.2. *Let the operator Λ be the difference of the Dirichlet-to-Neumann maps with respect to the Dirichlet data $h[dr] := drr^\star(\partial v/\partial \mathbf{n})|_\Gamma$*

$$\Lambda(h[dr]) := \frac{\partial dw[dr]}{\partial \mathbf{n}}\Big|_\Gamma - \frac{\partial dv[dr]}{\partial \mathbf{n}}\Big|_\Gamma.$$

Then, Λ is compact as an operator $\Lambda : H^{1/2}(\Gamma) \to H^{-1/2}(\Gamma)$, i.e., in its natural trace spaces.

Proof. We conclude from (2.12) and (2.13)

$$\left[V_{\Gamma\Gamma} - K_{\Sigma\Gamma}(1/2 + K_{\Sigma\Sigma})^{-1}V_{\Gamma\Sigma}\right] \frac{\partial dv}{\partial \mathbf{n}}\Big|_\Gamma = \left[1/2 + K_{\Gamma\Gamma} - K_{\Sigma\Gamma}(1/2 + K_{\Sigma\Sigma})^{-1}K_{\Gamma\Sigma}\right] h,$$

$$\left[V_{\Gamma\Gamma} - V_{\Sigma\Gamma}V_{\Sigma\Sigma}^{-1}V_{\Gamma\Sigma}\right] \frac{\partial dw}{\partial \mathbf{n}}\Big|_\Gamma = \left[1/2 + K_{\Gamma\Gamma} - V_{\Sigma\Gamma}V_{\Sigma\Sigma}^{-1}K_{\Gamma\Sigma}\right] h.$$

Since in both equations the operators on the left as well as on the right hand side are invertible and their difference is compact, we conclude

$$A\frac{\partial dv}{\partial \mathbf{n}}\Big|_\Gamma = Bh, \qquad [A + \mathcal{C}_1]\frac{\partial dw}{\partial \mathbf{n}}\Big|_\Gamma = [B + \mathcal{C}_2]\, h,$$

where A and B are bijective and continuous and $\mathcal{C}_1$ and $\mathcal{C}_2$ are compact perturbations in the associated spaces. Therefore we arrive at

$$\frac{\partial dw}{\partial \mathbf{n}}\Big|_\Gamma - \frac{\partial dv}{\partial \mathbf{n}}\Big|_\Gamma = \left[(A + \mathcal{C}_1)^{-1}(B + \mathcal{C}_2) - A^{-1}B\right] h$$

which is the desired result, since

$$(A + \mathcal{C}_1)^{-1}(B + \mathcal{C}_2) - A^{-1}B = (A + \mathcal{C}_1)^{-1}\mathcal{C}_2 + \left[(A + \mathcal{C}_1)^{-1} - A^{-1}\right] B$$

is compact. □

In order to illustrate the compact behaviour of the operator Λ we consider an analytic example concerning the situation of a ringshaped domain given by two concentric circles.

Example 2.3. *Let $D = B_1(\mathbf{0}) \subset \mathbb{R}^2$ be the unit circle and $S = B_R(\mathbf{0})$ for some $0 < R < 1$. Then we have $\Omega = D \setminus S := \{(\rho, \varphi) : \rho \in (R, 1),\ \varphi \in [0, 2\pi)\}$, $\Sigma = \{(\rho, \varphi) : \rho = 1,\ \varphi \in [0, 2\pi)\}$, and $\Gamma = \{(\rho, \varphi) : \rho = R,\ \varphi \in [0, 2\pi)\}$. Harmonic functions on such ringshaped domains can be represented via an ansatz in polar coordinates*

$$u(\rho, \varphi) = A_0 + B_0 \log \rho + \sum_{n=1}^{\infty} \left(A_n \rho^n + \frac{A_{-n}}{\rho^n} \right) \cos n\varphi + \left(B_n \rho^n + \frac{B_{-n}}{\rho^n} \right) \sin n\varphi.$$

Expanding the Dirichlet data $h = dv|_\Gamma = dw|_\Gamma$ in a Fourier series

$$h = h_0 + \sum_{n=1}^{\infty} h_n \cos n\varphi + h_{-n} \sin n\varphi,$$

and observing the boundary condition $dw|_\Sigma = 0$, we arrive at

$$dw(\rho, \varphi) = h_0 \frac{\log \rho}{\log R} + \sum_{n=1}^{\infty} \frac{R^n}{1 - R^{2n}} \left(\frac{1}{\rho^n} - \rho^n \right) (h_n \cos n\varphi + h_{-n} \sin n\varphi).$$

Similarly, from $(\partial dv / \partial \mathbf{n})|_\Sigma = (\partial dv / \partial \rho)|_{\rho=1} = 0$, we conclude

$$dv(\rho, \varphi) = h_0 + \sum_{n=1}^{\infty} \frac{R^n}{1 + R^{2n}} \left(\frac{1}{\rho^n} + \rho^n \right) (h_n \cos n\varphi + h_{-n} \sin n\varphi).$$

Employing $(\partial dw / \partial \mathbf{n})|_\Gamma = -(\partial dw / \partial \rho)|_{\rho=R}$ and likewise for dv, we find

$$\frac{\partial dw}{\partial \mathbf{n}}\Big|_\Gamma - \frac{\partial dv}{\partial \mathbf{n}}\Big|_\Gamma = \frac{h_0}{R \log R} - 4 \sum_{n=1}^{\infty} \frac{n R^{2n-1}}{1 - R^{4n}} (h_n \cos n\varphi + h_{-n} \sin n\varphi).$$

The exponential decay of the resulting Fourier coefficients clearly indicates the compactness of the map Λ. Moreover, the decay is the faster the smaller the radius R of the inclusion.

According to the Lemmas 2.1 and 2.2, the bilinear form $d^2 J(\Omega^\star)$ defined in (2.15) is continuous on $H^{1/2}(\Gamma) \times H^{1/2}(\Gamma)$. Hence, it represents a continuous linear operator

$$H = 2M^\star \Lambda M : H^{1/2}(\Gamma) \to H^{-1/2}(\Gamma)$$

As an immediate consequence of our considerations we conclude the following proposition.

Proposition 2.4. *The shape Hessian $H : H^{1/2}(\Gamma) \to H^{-1/2}(\Gamma)$ is compact at the optimal domain $\Omega^\star$.*

Remark 2.5. *The domain $\Omega^\star$ is a strict local minimizer of (1.2) if*

$$J(\Omega) > J(\Omega^\star) = 0, \quad \textit{for all } \Omega \subset U_\delta(\Omega^\star).$$

Nevertheless, a regular strict minimizer of second order satisfies $H^{1/2}$-coercivity of the shape Hessian

$$d^2 J(\Omega^\star)[dr, dr] \geq c\|dr\|^2_{H^{1/2}(\Gamma)},$$

cf. Dambrine and Pierre [4, 5]. *The above proposition implies immediately that this sufficient second order optimality condition is not satisfied.*

The above considerations specify no detailed information on the eigenvalues of the shape Hessian. We show in two examples that the eigenvalues of the shape Hessian decrease *exponentially*. The first example given below is computed analytically. The second one, concerned with the constellation in Figure 1.1, is presented in Section 4, where we compute the eigenvalues numerically. Despite the fact that we have not introduced any finite dimensional approximation of the minimization problem yet, we have to keep in mind exponentially growing condition numbers of the discrete shape Hessian when increasing the degrees of freedom.

Example 2.6. *We consider the same configuration as in Example 2.3, i.e.,* $\Omega = \{(\rho, \varphi) : \rho \in (R, 1),\ \varphi \in [0, 2\pi)\}$. *If we choose for example the Dirichlet data* $f := (x^2 - y^2)|_{\rho=1} = \cos 2\varphi$ *we conclude* $g = 2(1+R^4)/(1-R^4)\cos\varphi$ *and* $(\partial v/\partial \mathbf{n})|_\Gamma = (\partial w/\partial \mathbf{n})|_\Gamma = -4R/(1-R^4)\cos\varphi$. *Straightforward calculation leads to*

$$\begin{aligned} d^2 J(\Omega^\star)[\cos k\varphi, \cos l\varphi] &= d^2 J(\Omega^\star)[\sin k\varphi, \sin l\varphi] \\ &= \begin{cases} \frac{32R^4\pi}{(1-R^4)^2}\left[\frac{(k-2)R^{2k-4}}{1-R^{4k-8}} + \frac{(k+2)R^{2k+4}}{1-R^{4k+8}}\right], & \text{if } k = l > 2, \\ \frac{32R^4\pi}{(1-R^4)^2}\frac{(k+2)R^{2k+4}}{1-R^{4k+8}}, & \text{if } |k-l| = 4 \text{ and } k, l > 2, \\ 0, & \text{if } |k-l| \neq 0, 4 \text{ and } k, l > 2. \end{cases} \end{aligned}$$

and $d^2 J(\Omega^\star)[\cos k\varphi, \sin l\varphi] = 0$ *for all* $k, l > 2$. *Consequently, the shape Hessian is a banded matrix with coefficients exhibiting an exponential decay with respect to higher frequencies.*

3. Discretization

3.1. **Finite dimensional approximation of boundaries.** Since the infinite dimensional optimization problem cannot be solved directly, we replace it by a finite dimensional problem. Based on polar coordinates, we can express the smooth function $r \in C^{2,\alpha}_{\text{per}}([0, 2\pi])$ by the Fourier series

$$r(\phi) = a_0 + \sum_{n=1}^{\infty} a_n \cos n\phi + a_{-n} \sin n\phi.$$

Hence, it is reasonable to approximate the radial function by a truncated Fourier series

$$r_{N_r}(\phi) = a_0 + \sum_{n=1}^{N_r} a_n \cos n\phi + a_{-n} \sin n\phi. \tag{3.16}$$

If r is analytical, the Fourier series r_{N_r} converges to r exponentially in N_r, which means, r_{N_r} is a p-approximation of r.

Since r_{N_r} admits $2N_r + 1$ degrees of freedom $a_{-N_r}, a_{1-N_r}, \ldots, a_{N_r}$, we arrive at a finite dimensional optimization problem in the open set

$$A_{N_r} := \{a_{-N_r}, a_{1-N_r}, \ldots, a_{N_r} \in \mathbb{R} : r_{N_r}(\phi) > 0,\ \phi \in [0, 2\pi]\} \subset \mathbb{R}^{2N_r+1}.$$

Hence, via the identification $r_{N_r} \Leftrightarrow \Omega_{N_r}$, the finite dimensional approximation of shape minimization problem (1.2) reads as

$$J(\Omega_{N_r}) \to \min. \tag{3.17}$$

The associated gradients and Hessians have to be computed with respect to all directions $dr, dr_1, dr_2 = \cos N_r\phi, \cos(N_r - 1)\phi, \ldots, \sin(N_r - 1)\phi, \sin N_r\phi$.

3.2. **Treating the optimization problem.** The minimization problem defined by (3.17) implies to find its stationary points $\Omega^\star_{N_r}$

$$dJ(\Omega^\star_{N_r})[dr] = 0 \tag{3.18}$$

for all directions $dr \in \{\cos N_r\phi, \cos(N_r - 1)\phi, \ldots, \sin(N_r - 1)\phi, \sin N_r\phi\}$.

To solve (3.18), we consider on the hand a method which is based only on first order information, namely a quasi Newton method updated by the inverse BFGS-rule without damping, see [13, 14] for the details.

On the other hand, we perorm a Newton method which we regularize since the shape Hessian is compact at the optimal domain $\Omega^\star$. Namely, abbreviating the discrete gradient by $\mathbf{G}_n$ and the associated Hessian by $\mathbf{H}_n$, we consider in the n-th iteration step the descent direction

$$\mathbf{h}_n := -(\mathbf{H}_n^2 + \alpha_n \mathbf{I})^{-1} \mathbf{H}_n \mathbf{G}_n,$$

where $\alpha_n > 0$ is an appropriately chosen regularization parameter. This descent direction $\mathbf{h}_n$ solves the minimization problem

$$\|\mathbf{H}_n\mathbf{h} - \mathbf{G}_n\|^2 + \alpha\|\mathbf{h}\|^2 \to \min$$

and corresponds to a Tikhinov regularization of equation (3.18). Moreover, note that we employ in both methods a quadratic line search with respect to the functional (1.2).

3.3. **Numerical method to compute the state.** Observing the formulas (1.2), (1.7) and (1.9), the functional, its gradient as well as its Hessian can be computed from the knowledge of the boundary data of the sate equations (1.1) and (1.4). These data are given by the boundary integral equations (2.10)–(2.13). Hence, it is rather convenient to employ a boundary element method to compute the required boundary data of the state equations. We use a Galerkin discretization by N_Φ piecewise linear functions $\{\theta_i^\Phi\}_{i=1}^{N_\Phi}$ on each boundary $\Phi \in \{\Sigma, \Gamma\}$. For $\Phi, \Psi \in \{\Sigma, \Gamma\}$, we introduce the system matrices

$$\mathbf{V}_{\Phi\Psi} = -\frac{1}{2\pi}\left[\int_\Psi \int_\Phi \log\|\mathbf{x}-\mathbf{y}\|\theta_i^\Phi(\mathbf{y})\theta_j^\Psi(\mathbf{x})d\sigma_\mathbf{y}d\sigma_\mathbf{x}\right]_{i=1,\ldots,N_\Phi,\, j=1,\ldots,N_\Psi},$$

$$\mathbf{K}_{\Phi\Psi} = \frac{1}{2\pi}\left[\int_\Psi \int_\Phi \frac{\langle \mathbf{x}-\mathbf{y}, \mathbf{n}_\mathbf{y}\rangle}{\|\mathbf{x}-\mathbf{y}\|^2}\theta_i^\Phi(\mathbf{y})\theta_j^\Psi(\mathbf{x})d\sigma_\mathbf{y}d\sigma_\mathbf{x}\right]_{i=1,\ldots,N_\Phi,\, j=1,\ldots,N_\Psi},$$

and the mass matrices

$$\mathbf{M}_\Phi = \left[\int_\Phi \theta_i^\Phi(\mathbf{x})\theta_j^\Phi(\mathbf{x})d\sigma_\mathbf{x}\right]_{i,j=1,\ldots,N_\Phi},$$

and the load vectors of Dirichlet data f_Φ and Neumann data g_Φ

$$\mathbf{f}_\Phi = \left[\int_\Phi \theta_i^\Phi(\mathbf{x})f(\mathbf{x})d\sigma_\mathbf{x}\right]_{i=1,\ldots,N_\Phi}, \qquad \mathbf{g}_\Phi = \left[\int_\Phi \theta_i^\Phi(\mathbf{x})g(\mathbf{x})d\sigma_\mathbf{x}\right]_{i=1,\ldots,N_\Phi}.$$

Then, the linear system of equations

$$\begin{bmatrix} \mathbf{V}_{\Gamma\Gamma} & \mathbf{V}_{\Sigma\Gamma} \\ \mathbf{V}_{\Gamma\Sigma} & \mathbf{V}_{\Sigma\Sigma} \end{bmatrix}\begin{bmatrix} \mathbf{a}_\Gamma \\ \mathbf{a}_\Sigma \end{bmatrix} = \begin{bmatrix} 1/2\mathbf{M}_\Gamma + \mathbf{K}_{\Gamma\Gamma} & \mathbf{K}_{\Sigma\Gamma} \\ \mathbf{K}_{\Gamma\Sigma} & 1/2\mathbf{M}_\Sigma + \mathbf{K}_{\Sigma\Sigma} \end{bmatrix}\begin{bmatrix} \mathbf{M}_\Gamma^{-1}\mathbf{f}_\Gamma \\ \mathbf{M}_\Sigma^{-1}\mathbf{f}_\Sigma \end{bmatrix}, \tag{3.19}$$

gives us the Neumann data $a_\Gamma = \sum_{i=1}^{N_\Gamma}[\mathbf{a}_\Gamma]_i\theta_i^\Gamma$ on Γ and $a_\Sigma = \sum_{i=1}^{N_\Sigma}[\mathbf{a}_\Sigma]_i\theta_i^\Sigma$ on Σ from the Dirichlet data on Γ and Σ. Likewise, the system

$$\begin{bmatrix} \mathbf{V}_{\Gamma\Gamma} & -\mathbf{K}_{\Sigma\Gamma} \\ -\mathbf{V}_{\Gamma\Sigma} & 1/2\mathbf{M}_\Sigma + \mathbf{K}_{\Sigma\Sigma} \end{bmatrix}\begin{bmatrix} \mathbf{b}_\Gamma \\ \mathbf{a}_\Gamma \end{bmatrix} = \begin{bmatrix} 1/2\mathbf{M}_\Gamma + \mathbf{K}_{\Gamma\Gamma} & -\mathbf{V}_{\Sigma\Gamma} \\ -\mathbf{K}_{\Gamma\Sigma} & \mathbf{V}_{\Sigma\Sigma} \end{bmatrix}\begin{bmatrix} \mathbf{M}_\Gamma^{-1}\mathbf{g}_\Gamma \\ \mathbf{M}_\Sigma^{-1}\mathbf{f}_\Sigma \end{bmatrix}, \tag{3.20}$$

yields the Dirichlet data $b_\Gamma = \sum_{i=1}^{N_\Gamma}[\mathbf{b}_\Gamma]_i\theta_i^\Gamma$ on Γ and the Neumann data $a_\Sigma = \sum_{i=1}^{N_\Sigma}[\mathbf{a}_\Sigma]_i\theta_i^\Sigma$ on Σ from the Neumann data $\mathbf{g}_\Gamma$ on Γ and the Dirichlet data $\mathbf{f}_\Sigma$ on Σ. The variables $\left(\partial^2 v/(\partial\mathbf{n}\partial\mathbf{t})\right)\big|_\Gamma$ and $\left(\partial^2 w/(\partial\mathbf{n}\partial\mathbf{t})\right)\big|_\Gamma$, required for the shape Hessian, can be computed by differentiating the piecewise linear representations of $(\partial v/\partial\mathbf{n})|_\Gamma$ and $(\partial w/\partial\mathbf{n})|_\Gamma$, respectively.

We mention that the appearing system matrices have to be computed only once for each domain while the systems (3.19) and (3.20) have to be solved very often with different right hand sides to obtain the local shape derivatives. Hence, we recommend to use a *wavelet Galerkin scheme* which yields quasi sparse system matrices. We refer to [8, 9, 10, 11] for more details on the wavelet based fast solution of boundary integral equations appearing in shape optimization.

4. Numerical results

4.1. **Quasi Newton versus regularized Newton method.** In our first example we consider the situation depicted in Figure 1.1, i.e., we choose the ellipse with semi-axes 0.45 and 0.3 as domain D. The inclusion centered in $\mathbf{x} = (0,0)^T$ is described by 15 Fourier coefficients. The Dirichlet data on $\Sigma = \partial D$ are chosen as $f = (x^2 - y^2)|_\Sigma$ while the Neumann data g on Σ are computed numerically with high accuracy.

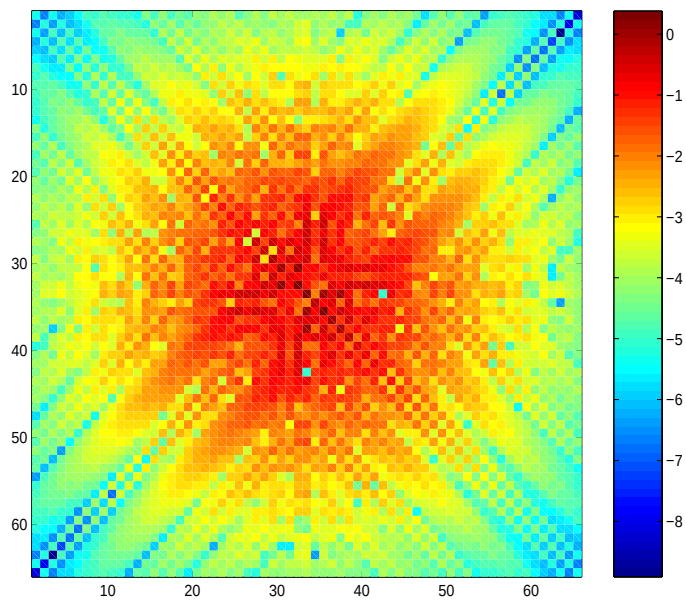

Figure 4.2. Logarithmic moduli of the coefficients of the discrete Hessian $d^2 J(\Omega^\star)[dr_1, dr_2]$.

The Hessian $d^2 J(\Omega^\star)[dr_1, dr_2]$ discretized via 65 Fourier coefficients ($N_r = 32$) is visualized in Figure 4.2. A plot of its eigenvalue distribution can be found in Figure 4.3. We mention that the first 16 eigenvalues are smaller than zero which issues from numerical roundoff errors, even though we applied $N_\Gamma = N_\Sigma = 1024$ boundary elements. The plot exhibits clearly the exponential decay of the eigenvalues. The ℓ^2-condition number of the discrete Hessian is about 10^9.

We employ the circle of radius 0.25 indicated by the dashed line in Figure 4.4 as initial guess in our regularized Newton method. It turns out that setting $\alpha_n = 2^{-n}$ in the n-th step of the regularized Newton method is the best choice of the regularization parameter. Thus, in each step we reduce the regularization parameter by the factor 2. We observe that, similarly to multiscale methods, in the first steps the low frequencies of the boundary are approximated while more and more the high frequencies are resolved during the iteration. Let us mention that the line search

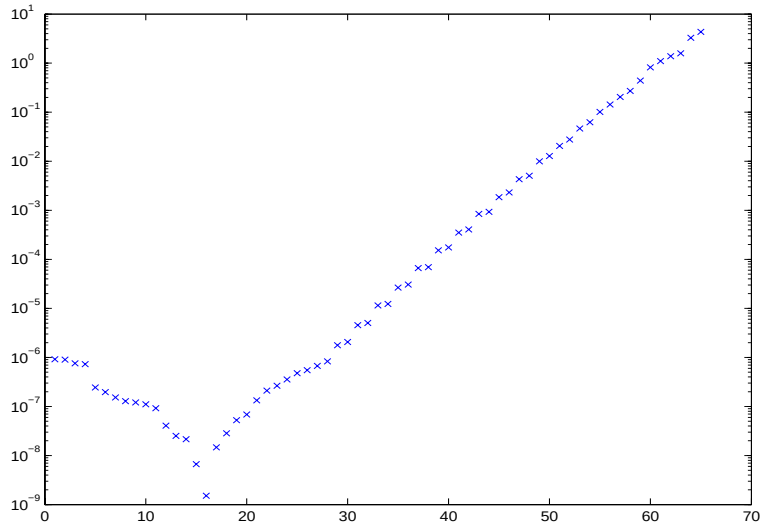

FIGURE 4.3. The eigenvalues of the discrete Hessian.

prevents the divergence of the method, particularly in the last iteration steps. The dash-dotted line in the right plot of Figure 4.4 indicates the solution in the case of 33 Fourier coefficients ($N_r = 16$) obtained after 50 steps of the regularized Newton method using 512 boundary elements on each boundary ($N_\Gamma = N_\Sigma = 512$). The right plot contains the solution after 50 steps of the quasi Newton method.

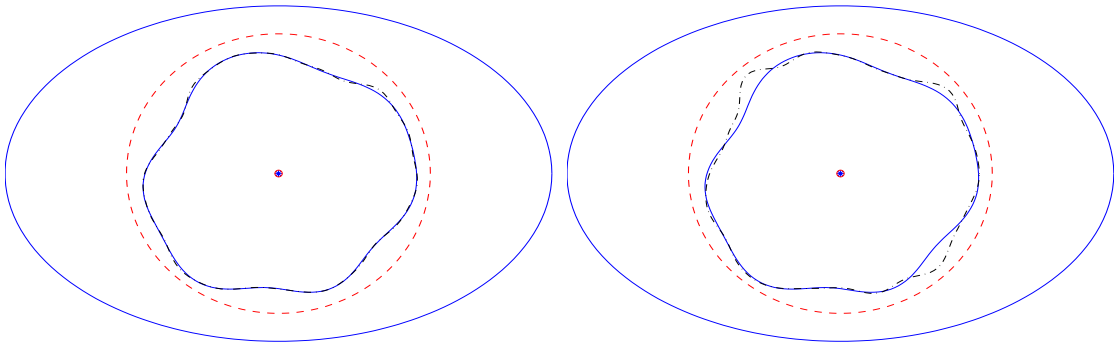

FIGURE 4.4. Initial guess and final approximation of the inclusion for 33 Fourier coefficients in case of the regularized Newton method (left) and the quasi Newton method (right).

The progress of the minimization of the shape functional during the iteration and the corresponding shape approximation errors measured by the ℓ^2-norm of the Fourier coefficients are plotted in Figure 4.5. The solid and dashed lines correspond to the regularized Newton and quasi Newton method, respectively. One observes faster convergence and higher accuracy for the regularized Newton scheme. In particular,

one recognizes from the plot concerning the functional that the objective is $2.8 \cdot 10^{-3}$ in the case of the initial guess and $3.5 \cdot 10^{-11}$ in the last step.

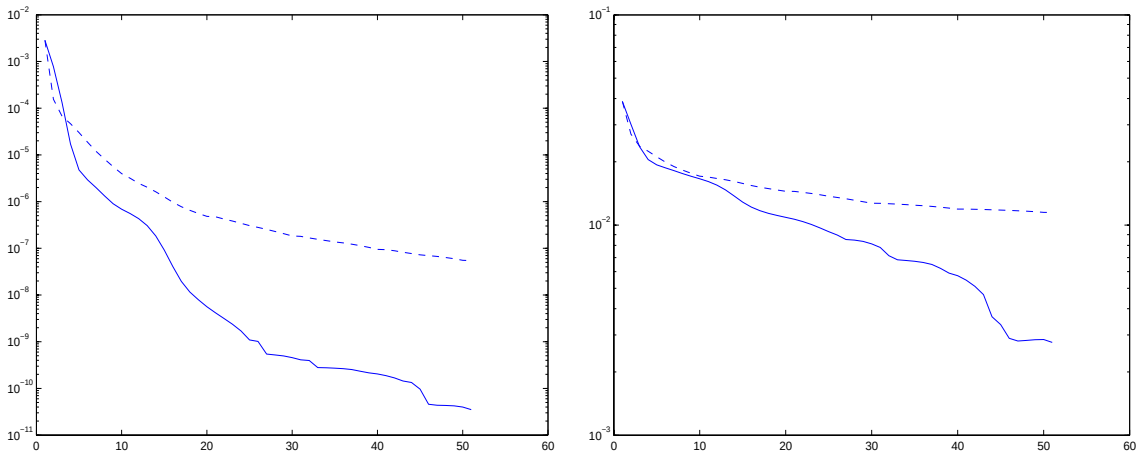

FIGURE 4.5. The values of the shape functional (left) and the ℓ^2-norm of the shape approximation errors (right).

Figures 4.4 and 4.5 confirm that the regularized Newton method computes the given inclusion more exact than the quasi Newton method.

4.2. **Preprocessing: Detecting the barycenter.** To apply the shape calculus from Subsection 1.2 for a refined resolution of the interface, the position of the pole of the polar coordinate system has to be detected in advance. To our experience the determination of this pole should be combined with a first crude predetermination of the shape of the given inclusion.

From the general formula (1.5), for a constant shift field $\mathbf{V} \equiv \mathbf{a}$ we derive the directional derivatives

$$dJ[\mathbf{a}] = \int_\Gamma \langle \mathbf{a}, \mathbf{n} \rangle \left[\left(\frac{\partial v}{\partial \mathbf{n}} \right)^2 - \left(\frac{\partial w}{\partial \mathbf{n}} \right)^2 \right] d\sigma = \left\langle \mathbf{a}, \int_\Gamma \mathbf{n} \left[\left(\frac{\partial v}{\partial \mathbf{n}} \right)^2 - \left(\frac{\partial w}{\partial \mathbf{n}} \right)^2 \right] d\sigma \right\rangle .$$

Based on these directional derivatives, the implementation of a first order optimization algorithm is straightforward.

We choose the same setup as in the first example but consider a lengthy inclusion centered in $\mathbf{x} = (0.1, 0)$, cf. Figure 4.6. The preprocessing step performed with the best fitting circle does not yield satisfying results since the circle is placed too close to the right boundary, cf. Figure 4.6 (dashed line). Neither first nor second order optimization methods detect the left boundary if this circle is used as initial guess for a refined resolution of the boundary (dash-dotted line).

Hence, we should consider more degrees of freedom with respect to the boundary. To ensure that the pole is equal to the barycenter, the radial function shall fulfill

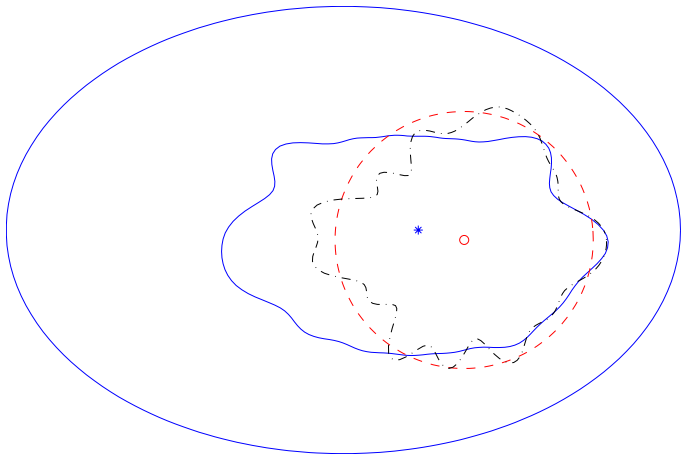

FIGURE 4.6. Approximation of the inclusion for the best fitting ball.

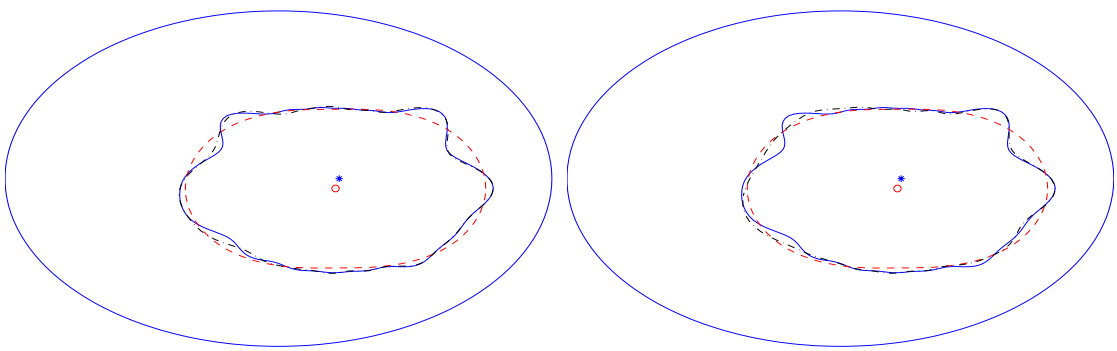

FIGURE 4.7. Preprocessing using B-splines and final approximation using the regularized Newton method (left) and the quasi Newton method (right).

$r(\varphi) = r(\varphi + \pi)$. In our experience, the best choice to get a crude approximation of the shape is the use of periodic cubic splines. We subdivide the interval $[0, 2\pi)$ equidistantly into 8 intervals and denote the smoothest n-th 2π-periodic cardinal B-spline of order 3 on the given partitioning by B_n^3. The ansatz $r(\varphi) = \sum_{n=1}^{8} b_n B_n^3(\phi)$ yields the conditions $b_n = b_{n+4}$ to ensure $r(\varphi) = r(\varphi+\pi)$. Hence, we have to consider the four directions $dr = B_n^3 + B_{n+4}^3$ in addition to the shift fields $\mathbf{a} = [1, 0]^T, [0, 1]^T$. This are six degrees of freedom which we minimized in the preprocessing step. The result of this preprocessing is indicated by dashed line in Figure 4.7.

The final approximation via 33 Fourier coefficients and 30 iterations of the regularized Newton method is presented in the left plot Figure 4.7. The plot on the right hand side shows the final approximation in case of 50 quasi Newton iterations. Again, the regularized Newton method resolves the inclusion more exact, particularly the left part its boundary. We remark that after the 45th iteration step of the

regularized Newton method the ℓ^2-condition number of the Hessian is greater than 10^{16}.

In both calculations, the preprocessing has been performed by 30 iteration steps of a quasi Newton method updated by the inverse BFGS-rule without damping, where the initial guess has been the circle of radius 0.1 and midpoint $(0,0)$. We mention that only a few boundary elements are required for the preprocessing. In fact, we have chosen $N_\Gamma = N_\Sigma = 64$. For the refined resolution of the boundary we have set $\alpha_n = 2^{-n}$ and $N_\Gamma = N_\Sigma = 512$.

4.3. **Scaling the inclusion.** In our last example we employ again the setup of the previous subsections but consider different scaled inclusions centered in $(-0.1, -0.05)$. The preprocessing is performed like above by using B-splines and 30 quasi Newton iterations. We iterate 30 times the regularized Newton scheme setting $\alpha_n = 2^{-n}$ and $N_\Gamma = N_\Sigma = 512$. The solutions are presented in Figure 4.8. As these plots confirm, the resolution of the boundary seems to be the more inexact the smaller the inclusion is. Nevertheless, the results confirm stability of the regularized Newton method.

Compared to the solution of the quasi Newton method, the resolution of the inclusion is more precise. For example, in Figure 4.9, the solution obtained after 50 steps of the quasi Newton method is depicted. It corresponds to the right plot in the middle of Figure 4.8.

5. Conclusion

The present paper is concerned with second order methods for the identification of voids or inclusions. The problem under consideration is well known to be severely ill-posed. Since the shape Hessian is compact at the optimal domain, we propose a regularized Newton method for the resolution of the inclusion. Combined with a preprocessing step to detect the barycenter and a first crude approximation of the inclusion, the numerical results evince that the regularized Newton method resolves the given inclusion more exact than first order methods.

References

[1] G. Alessandrini, V. Isakov, and J. Powell Local uniqueness in the inverse problem with one measurement. *Trans. Am. Math. Soc.*, 347:3031–3041, 1995.

[2] M. Brühl. Explicit characterization of inclusions in electrical impedance tomography. SIAM J. Math. Anal. 32, no.6, 1327–1341, 2001.

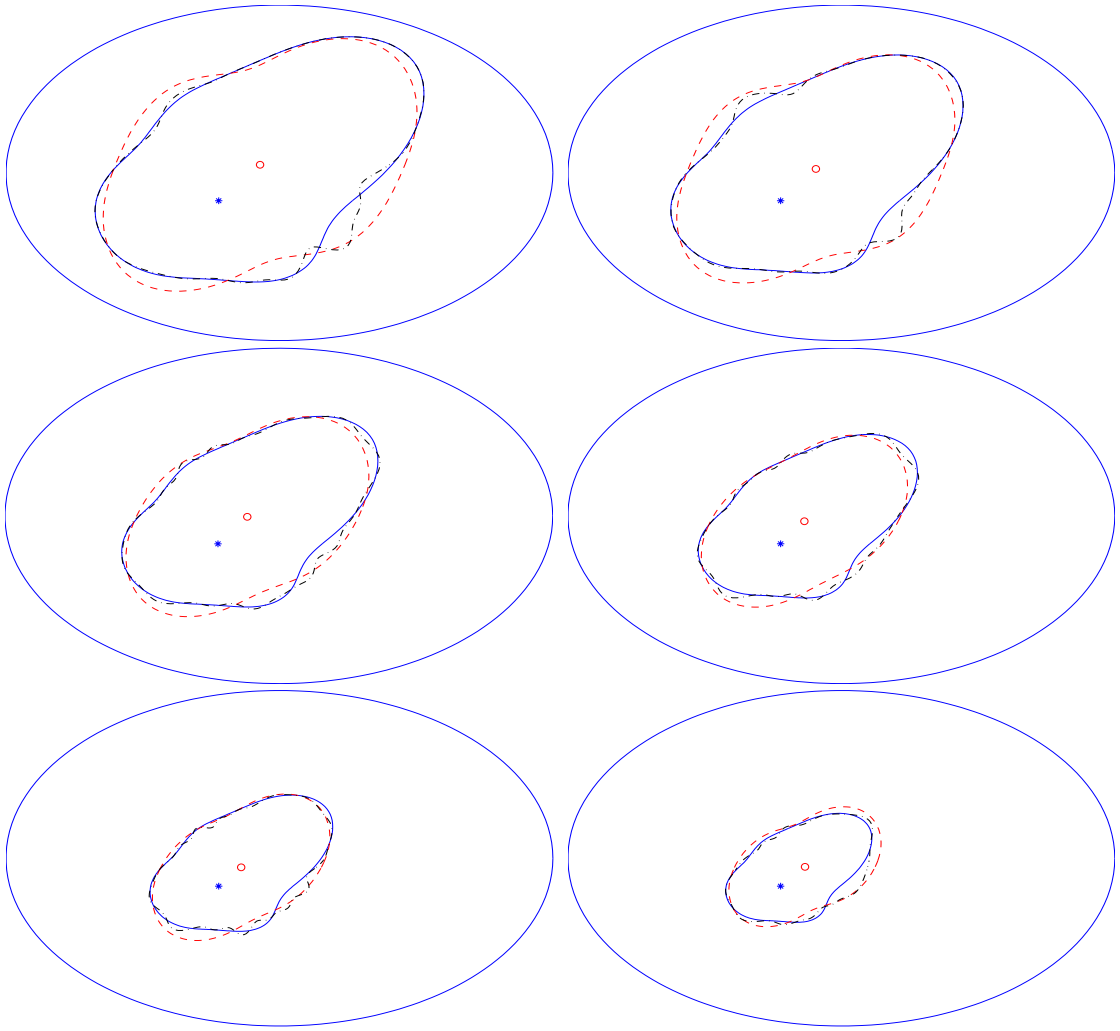

FIGURE 4.8. Preprocessing and final approximation by the regularized Newton method while reducing the size of the inclusion.

[3] M. Brühl and M. Hanke. Numerical implementation of two noniterative methods for locating inclusions by impedance tomography. Inverse Problems 16, no.4, 1029–1042, 2000.

[4] M. Dambrine and M. Pierre. About stability of equilibrium shapes. *M2AN* 34, No.4, 811–834, 2000.

[5] M. Dambrine. On variations of the shape Hessian and sufficient conditions for the stability of critical shapes. *RACSAM, Rev. R. Acad. Cien. Serie A. Mat.* 96, No.1, 95–121, 2002.

[6] K. Eppler Optimal shape design for elliptic equations via BIE-methods. *J. of Applied Mathematics and Computer Science* 10:487–516, 2000.

[7] K. Eppler. Boundary integral representations of second derivatives in shape optimization. *Discussiones Mathematicae (Differential Inclusion Control and Optimization)*, 20:63–78, 2000.

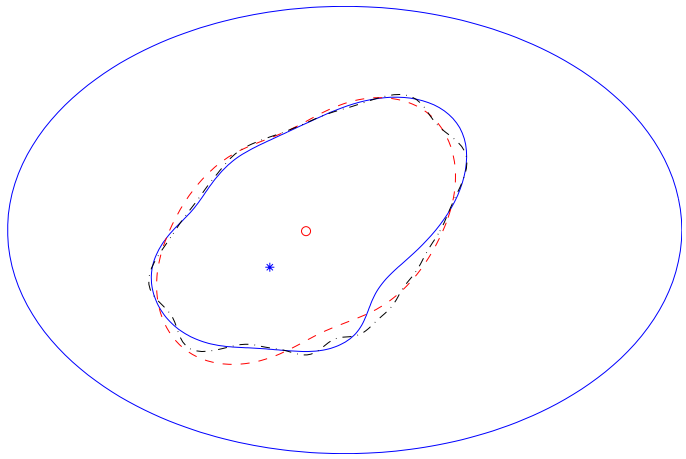

FIGURE 4.9. Approximation of the inclusion by the quasi Newton method.

[8] K. Eppler and H. Harbrecht. Numerical solution of elliptic shape optimization problems using wavelet-based BEM. *Optim. Methods Softw.*, 18:105–123, 2003.

[9] K. Eppler and H. Harbrecht. 2nd Order Shape Optimization using Wavelet BEM. *Preprint 06-2003, TU Berlin*, 2003. submitted to Optim. Methods Softw.

[10] K. Eppler and H. Harbrecht. Exterior Electromagnetic Shaping using Wavelet BEM. *Preprint 13-2003, TU Berlin*, 2003. to appear in Math. Meth. Appl. Sci.

[11] K. Eppler and H. Harbrecht. Fast wavelet BEM for 3d electromagnetic shaping. *Bericht 03-9*, Berichtsreihe des Mathematischen Seminars der Christian-Albrechts-Universitt zu Kiel, 2003. to appear in Appl. Numer. Math.

[12] A. Friedman and V. Isakov. On the uniqueness in the inverse conductivity problem with one measurement. *Indiana Univ. Math. J.*, 38:563–579, 1989.

[13] P.E. Gill, W. Murray and M.H. Wright. *Practical Optimization.* Academic Press, New York, 1981.

[14] Ch. Grossmann and J. Terno. *Numerik der Optimierung.*

[15] W. Hackbusch. *Integralgleichungen.* B.G. Teubner, Stuttgart, 1989.

[16] F. Hettlich and W. Rundell The determination of a discontinuity in a conductivity from a single boundary measurement. *Inverse Problems.* 14:67–82, 1998.

[17] G. Hsiao and W. Wendland. A finite element method for some equations of first kind. *J. Math. Anal. Appl.*, 58:449–481, 1977.

[18] R. Kress. *Linear Integral Equations.* Springer-Verlag, Berlin-Heidelberg, 1989.

[19] V.G. Maz'ya and T.O. Shaposhnikova. *Theory of multipliers in spaces of differentiable functions.* Pitman, Boston, 1985.(Monographs and Studies in Mathematics, 23. Pitman Advanced Publishing Program. Boston - London - Melbourne: Pitman Publishing Inc. *XIII*, 344 p. (1985))

[20] J.-R. Roche and J. Sokolowski Numerical methods for shape identification problems. *Control Cybern.* 25:867–894, 1996.

[21] J. Sokolowski and J.-P. Zolesio. *Introduction to Shape Optimization.* Springer, Berlin, 1992.

[22] H. Triebel *Theory of function spaces.* Birkhäuser, Basel-Boston-Stuttgart, 1983.